Journal of Hydroscience and Hydraulic Engineering
Vol. 8, No. 1, October, 1990, 9-30

AN ANALYTICAL SOLUTION FOR BUOYANCY-DRIVEN FLOW

by

Mookencheril P. Cherian and Subhash C. Jain
Iowa Institute of Hydraulic Research
The University of Iowa, Iowa City, Iowa, U.S.A.

SYNOPSIS

An analytical solution to the problem of the two-dimensional steady state buoyancy-driven flow in a sidearm of a cooling lake is obtained. The solution procedure involves integrating the governing equations over the depth of the sidearm using similarity profiles for the vertical temperature, velocity, and shear-stress distributions. The governing partial differential equations are reduced to a system of ordinary differential equations and solved analytically. The solution incorporates the laminar, quasi-laminar and turbulent regimes of flow. The closed-form solution yields the distribution of discharge and surface temperature along the sidearm. Good agreement between the model results and available laboratory and field data is obtained.

INTRODUCTION

Cooling lakes formed by impounding natural rivers are an attractive option for management of waste heat from steam-electric power plants. These lakes offer the advantages of high thermal inertia, low intake temperature, minimal maintenance and possible recreational value. Cooling lakes often have dead-end sidearms or cul-de-sacs because of the topography of the lake site. In many cooling lakes, sidearms represent a significant portion of the pond surface area. Although there is no net flow through these sidearms, they are effective heat transfer agents because of the longitudinal density gradients which produce density (buoyancy) currents that advect heat into them. Therefore, proper cooling lake design and analysis require that these buoyancy currents in sidearms be taken into account.

Physical Description

A detailed description of the physical processes at work in sidearms of cooling lakes is given by Sturm (1976), and a brief description is given here. Consider an idealized cooling-lake sidearm with variable depth D, horizontal bottom, and large length-to-depth ratio, as shown in figure 1. At the entrance to the sidearm, the water is density stratified as a result of thermal loading of the flow through the lake. Under the assumption that the vertical force balance is hydrostatic everywhere,

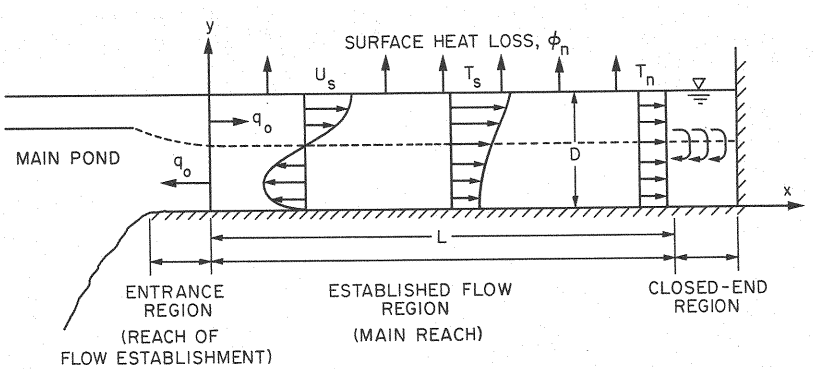

Figure 1. Definition Sketch.

$$\frac{\partial p}{\partial y} = -g\rho(x,y) \tag{1}$$

in which p is the pressure, ρ is the local water density and g is the acceleration due to gravity. Integration of Eq. 1 from an arbitrary y to D and differentiation of the result yields

$$\frac{\partial p}{\partial x} = g \int_{D}^{y} \frac{\partial \rho}{\partial x} dy + \rho_s(x)\ g \frac{dD}{dx} \tag{2}$$

in which ρ_s (x) is the surface density. The temperature decreases in the x-direction due to surface heat loss, and consequently the first term on the right-hand side of Eq. 2 is positive for all $0 \le y \le D$. Clearly, then, if flow continuity is to be maintained for steady state conditions, dD/dx must be negative so that the negative pressure gradient drives an inflow current in the top layers of the sidearm. At the lower levels where the density-gradient contribution dominates, the pressure gradient is positive and hence an outflow current is generated. If the arm is very long, the surface water temperature will decrease eventually to its equilibrium value T_e, the temperature at which there is no heat transfer across the water surface. The length of the sidearm at which the surface water temperature $T_s(x)$ decreases to T_e is defined as the equilibrium length, L_e. Sidearms of length $L > L_e$ and $L < L_e$ are referred to as long and short sidearms respectively. For long sidearms the active length for heat dissipation is the equilibrium length; the portion of the sidearm beyond the equilibrium length section does not contribute to cooling.

Three flow regions along a sidearm are distinguished; sequentially from the open end these are the reach of flow establishment, the main reach, and the closed-end reach. In the region of flow establishment, rapid changes in depth of the interface between the inflow and outflow currents may occur depending on the ratio of the depth of warm layer in the main pond to that of the depth of the sidearm. The governing forces in this region are those of inertia and buoyancy. The reach of flow establishment is normally quite short and hence for considerations of heat loss is not very significant. In the main reach the flow becomes nearly one dimensional. The dominant forces here are those of viscosity and buoyancy. As surface cooling reduces the temperature of the water in the x direction, the rate of surface cooling decreases which reduces the density gradients and hence also the inflow and outflow velocities. Consequently, along this reach there is flow exchange between the inflow and outflow currents. However, because of the strong density gradients that exist at the interface between the inflow and outflow currents, the flow exchange between the two layers per unit distance along the sidearm tends to be small. Therefore, for short sidearms, the flow exchange between the layers is relatively small and hence the temperatures along the outflow are practically constant. For long sidearms, the entire flow in the upper layer of the main reach is eventually converted into downflow and consequently there is significant temperature change along the outflow. The elevation of the interface along this reach of the sidearm remains practically constant. Application of the approximations of the boundary-layer type to the governing equations is valid in this region because the vertical velocities are small in comparison to a representative horizontal velocity and the diffusive momentum and heat fluxes are much stronger vertically than horizontally. Most of the surface heat loss from the sidearm usually occurs in this region of flow. In the closed-end reach of long sidearms the horizontal and vertical velocities are nearly zero and the temperature everywhere is close to T_e. For short sidearms, the inflow discharge at the beginning of the closed-end reach is abruptly deflected and reversed to initiate the outflow current in the lower layer and hence the temperature of the lower layer is nearly the same as that of the upper layer in this reach. Surface heat loss from this region is usually negligible.

Furthermore, experimental evidence indicates the existence of three regimes of sidearm flow: 1) a laminar regime with laminar flow conditions in both the upper and lower layers; 2) a quasi-laminar regime in which flow in the upper layer is turbulent due to surface cooling instability while flow in the lower layer is laminar; and 3) a turbulent regime in which flow in both layers is turbulent. Convective turbulence is present to some extent in all buoyancy flows sustained by surface cooling; quasi-laminar flow occurs only when the convective cells generated by surface cooling are strong enough to penetrate the entire upper layer and thereby alter the temperature and velocity distribution in the upper layer from the corresponding laminar profiles.

The distinction between the upper and lower layer, and hence the definition of the interface, is based, in this study, on the temperature/density distribution. The interface is defined as that layer/plane at which a distinct discontinuity in density takes place.

PREVIOUS RESEARCH

The earliest work on buoyancy-driven currents in lakes was carried out by Phillips (1966), who utilized similarity arguments and assumed a constant surface buoyancy flux to derive the functional dependence of the mean velocity and buoyancy on streamwise distance for turbulent convective flows in the Red Sea. Edinger (1971) presented a model based on the assumption of diffusion of heat into sidearms in order to evaluate the cooling performance of sidearms. Dresner (1973) applied the two-layer stratified flow equations to sidearms and developed a model in which friction was neglected and the thermal energy equation was uncoupled from the equations of motion. More recently, solutions to the depth-integrated governing equations have been presented.

Sturm (1976) obtained a closed-form solution for the case of laminar flow by neglecting the inertia term and the water-surface slope. Sturm (1981) improved on his earlier solution by including the slope term in his analysis. Sturm and Kennedy (1980) obtained a numerical solution without neglecting any terms and presented the results in graphical form. Jain (1982) neglected the water-surface slope in his analytical analysis. Brocard et al. (1977) used a two-layer approach to the sidearm circulation problem. The governing partial differential equations were integrated vertically for each side of the interface to obtain a system of equations for each flow layer. The integrated equations then were expressed in terms of flow rates and vertically-averaged densities in each layer. An order of magnitude analysis indicated that the water-surface slope was much smaller than the interfacial slope, and hence was neglected in comparison to the interfacial slope. Although the general formulation included a number of variable input parameters, the closed-form solution of interest neglected the bottom slope and interfacial heat transfer and assumed zero flux of water across the interface. The neglect of flow exchange between the two layers is a limitation of this model; clearly, downflow is significant in long sidearms and cannot be neglected.

The following conclusions can be drawn from an examination of the numerical and analytical studies summarized above. For models in which the governing equations are integrated over the entire depth of flow, the water-surface slope is a major contributor to the balance of forces in the integrated momentum equation and cannot be neglected. In such models, the inertia term in the integrated momentum equation is negligible for laminar flow under laboratory conditions. For models in which the governing equations are integrated over the layer depths, the water-surface slope is small in comparison to the interfacial slope, and can be neglected. Integral momentum analysis then shows that the inertia term plays a vital role in the integrated momentum equation. Flow exchange between the upper and lower layers cannot be neglected.

Experimental investigations also were carried out by Sturm (1976) and Brocard et al. (1977). The temperature and velocity profiles obtained by Sturm displayed laminar characteristics. The Reynolds number, R, in his experiments was about 200; $R = q/\upsilon$ in which q is the discharge per unit width of the sidearm and υ is the kinematic viscosity of water. In the experiments of Brocard et al., the temperature profiles exhibited a vertically well-mixed upper layer, and a photograph of dye trace in the lower layer showed a parabolic velocity distribution similar to that for a laminar flow between parabolic velocity distribution similar to that for a laminar flow between parallel plates; the Reynolds number varied between 250 and 1000; and the flow regime was quasi-laminar. The experimental results of Sturm and Brocard et al. also indicated that the sidearm circulation can be represented by a two-layer flow structure, and that the vertical profiles of temperature and velocity are similar.

A general model, capable of accurately predicting the cooling performance of a sidearm for all possible flow regimes, is lacking. The investigation in this paper was concentrated on developing such a model. The approach adopted in formulating the problem is the same as that of Sturm (1976); i.e., the governing equations are integrated over the entire depth of flow to yield the relevant one-dimensional equations. The disadvantage with the method proposed by Brocard et al. (1977) is that the flow exchange between the layers must be prescribed a priori; it cannot be obtained as a solution. An analytical solution is then obtained to the one-dimensional equations by making certain, well-justified, order of magnitude approximations. Use is made of the observations and results of past investigations to arrive at the closed-form solution.

REMARKS ON SOLUTION APPROACH

The integrated governing equations presented later contain three unknows; namely, longitudinal velocity component u; temperature T; and flow depth D. Because the integration of the differential form of the continuity equation over the flow depth becomes zero, the integrated continuity equation does not provide a relation among the unknowns. The closure problem is resolved by using the

mechanical-energy equation. The solution method of using the mechanical-energy equation in addition to the momentum equation is similar to the "integral dissipation method" employed by many researchers to analyze boundary-layer flows. One often cited drawback of using both the momentum and mechanical-energy equations is that the two equations are not independent. Though the two equations in the differential form do not offer independent information, these two equations in the integral form do provide independent information because the information lost in the integration differs for the two equations (Reynolds 1968). The performance of the integral dissipation methods based on the mechanical-energy equation was judged to be "good" by the Evaluation Committee of the AFOSR-IFP-Standard Conference on "Computation of turbulent boundary layers: (Kline et al. 1968)); one entire session of the conference, which included seven papers, was devoted to the integral dissipation methods. Sturm and Kennedy (1980) successfully used this approach to obtain a numerical solution of density currents in sidearms. The satisfactory agreement between the analytical results and experimental data included in the present study further corroborate the validity of the adopted solution method.

ANALYTICAL FORMULATION

Governing Equations

The governing equations for steady-state motion in the fully-established flow region of the sidearm are formulated using the boundary-layer approximations and Boussinesq's approximation.

$$\frac{\partial u}{\partial x}+\frac{\partial v}{\partial y}=0 \text{ (continuity)} \tag{3}$$

$$u\frac{\partial u}{\partial x}+v\frac{\partial u}{\partial y}=-\frac{1}{\rho_n}\frac{\partial p}{\partial x}+\frac{1}{\rho_n}\frac{\partial \tau_{xy}}{\partial y} \text{ (x-momentum)} \tag{4}$$

$$0=-\frac{\partial p}{\partial y}-\rho g \text{ (y-momentum)} \tag{5}$$

$$u\frac{\partial T}{\partial x}+v\frac{\partial T}{\partial y}=\frac{\partial}{\partial y}\left(D_y\frac{\partial T}{\partial y}\right) \text{ (thermal energy)} \tag{6}$$

$$\rho=-\beta\rho_n T+\alpha \text{ (state)} \tag{7}$$

in which u and v are the components of the velocity vector in the x- and y- directions, respectively; p is the pressure; T is the temperature; ρ_n is a reference density of water, which is taken as the density of water corresponding to the temperature at the end of the sidearm; β is the coefficient of thermal expansion of water; α is a constant; τ_{xy} is the shear stress; and D_y is the thermal diffusivity. Turbulence, though not considered explicitly, is accounted for by treating the velocity and temperature variables in Eqs. 3 to 7 as time-averaged variables, by including the Reynolds shear stress in the stress term τ_{xy}, and by including both the molecular and turbulent diffusion coefficients in D_y.

The boundary conditions for Eqs. 3 to 7 are

$$x=0;\ T=g(y) \tag{8}$$

$$x=0;\ \int_0^D u\,dy=0 \tag{9}$$

$$y=0;\ \frac{\partial T}{\partial y}=0,\ u=0,\ v=0 \tag{10}$$

$$y = D;\ D_y \frac{\partial T}{\partial y} = \frac{\phi_n}{\rho_n c_p},\ \frac{\partial u}{\partial y} = 0,\ p = 0 \tag{11}$$

in which g(y) is the vertical temperature distribution at $x = 0$; ϕ_n is the rate of heat transfer across the water surface; c_p is the specific heat of water; and D is the sidearm flow depth.

Integrated Governing Equations

Elimination of the pressure term between Eqs. 4 and 5, integration of the continuity, momentum and energy equations over the flow depth D and application of the appropriate boundary conditions produce

$$\int_0^D u\, dy = \text{constant} = 0 \tag{12}$$

$$\frac{d}{dx}\int_0^D u^2 dy = \frac{-g}{\rho_n}\frac{d}{dx}\left[\int_0^D \int_y^D (-\beta\rho_n T + \alpha)\, dy\, dy\right] - \frac{\tau_o}{\rho_n} \tag{13}$$

$$\frac{d}{dx}\int_0^D u\, T\, dy = \frac{\phi_n}{\rho_n c_p} \tag{14}$$

in which τ_o is the shear stress at the channel bottom. Eq. 12 is a generalized form of the boundary condition, Eq. 9.

In the following treatment, D is considered as a function of x, D(x). Consequently, the principal integrated governing equations, 13 and 14, now contain an additional unknown D(x). To resolve the problem of closure an additional equation, the mechanical energy equation, is generated by multiplying the x and y equations of motion, Eqs. 4 and 5 by u and v, respectively and adding the results (see earlier section for justification). The integrated mechanical energy equation is written as

$$\int_0^{D(x)} \left(u^2 \frac{\partial u}{\partial x} + uv \frac{\partial u}{\partial y}\right) dy = -\frac{1}{\rho_n}\int_0^{D(x)} \left(u \frac{\partial p}{\partial x} + v \frac{\partial p}{\partial y} + v\rho_n g\right) dy$$

$$+ \frac{1}{\rho_n}\int_0^{D(x)} u \frac{\partial \tau_{xy}}{\partial y}\, dy \tag{15}$$

Eq. 15 can be further simplified to

$$\frac{1}{2}\frac{d}{dx}\int_0^{D(x)} u^3 dy = -\frac{1}{\rho_n}\int_0^{D(x)} u \frac{\partial p}{\partial x} dy + \frac{1}{\rho_n}\int_0^{D(x)} u \frac{\partial \tau_{xy}}{\partial y} dy \tag{16}$$

The additional boundary condition is

$$x = 0;\ D = D_o \tag{17}$$

where D_o is the sidearm flow depth at $x = 0$.

Reduction of the Integrated Equations

The first step in the solution of the governing equations involves reduction of the integrated equations 13, 14 and 16 to a system of ordinary differential equations. Utilizing the experimental evidence that the vertical profiles for velocity and temperature are similar and hence assuming that the

vertical profiles for shear stress are also similar, the following definitions for these profiles are adopted.

$$f(\eta) = \frac{u}{u_s}$$

$$h(\eta) = \frac{T-T_n}{T_s-T_n} \tag{18}$$

$$\bar{\tau}(\eta) = \frac{\tau}{|\tau_o|}$$

$$\eta = y/D$$

in which $f(\eta)$, $h(\eta)$ and $\bar{\tau}(\eta)$ are the normalized similarity profiles for velocity, temperature, and shear stress, respectively; u_s is the flow velocity at the water surface; T_s is the water-surface temperature; and T_n is the temperature at the end of the sidearm which is assumed uniform in the vertical direction. Note that T_n is, as yet, an unknown quantity. It is obtained, later, from the solution to the governing equations by imposing the condition that at

$$x = L, \; T = T_n \tag{19}$$

Certain conditions on the similarity profiles for velocity and temperature can now be obtained. Eq. 12 yields

$$\int_0^1 f(\eta) \, d\eta = 0 \tag{20}$$

Boundary condition, Eq. 10, demands

$$f(0) = 0 \tag{21}$$

Eq. 11 yields

$$\partial f/\partial \eta \big|_{\eta = 1} = 0 \tag{22}$$

From Eq. 18

$$f(1) = 1 \tag{23}$$

Conditions, Eqs. 20, 21, and 23, imply that at some $\eta = \Lambda_v$,

$$f(\Lambda_v) = 0 \tag{24}$$

where $\Lambda_v = h_v/D$, in which h_v is the elevation of the point of zero velocity. Note that, in general,

$$f(\Lambda_T) \neq 0 \tag{25}$$

where Λ_T is the normalized interface elevation given by h_T/D and h_T is the elevation of the interface measured from the channel bottom. Eqs. 20 to 24 are the conditions on the normalized vertical profile.

From experimental observation

$$h(0) = 0 \tag{26}$$

Eq. 10 yields

$$\frac{\partial h}{\partial \eta} = 0 \text{ at } \eta = 0 \tag{27}$$

Shear stress is zero at the free surface, and the interfacial shear stress (evaluated later) is τ_i; i.e.,

$$\bar{\tau}(1) = 0$$

$$\bar{\tau}(\Lambda_T) = \frac{\tau_i}{|\tau_o|} \tag{28}$$

$$\bar{\tau}(0) = 1$$

If the adopted similarity profiles satisfy conditions, Eqs. 20 to 28, the problem reduces to one of solving the integrated equations subject to the boundary conditions, Eqs. 8 and 17. The third boundary condition (for the velocity) is obtained as an internal condition as is shown later. The forms of the similarity profiles, $h(\eta)$, $f(\eta)$, and $\bar{\tau}(\eta)$ are also given in a later section.

On substitution of Eq. 18 in the momentum, mechanical-energy and thermal-energy equations, the following are obtained:

$$c_o \frac{d}{dx}(u_s^2 D) = c_1 \beta g \frac{d}{dx}[D^2(T_s - T_n)] - \frac{g}{2}\frac{dD^2}{dx} - \frac{\tau_o}{\rho_n} \tag{29}$$

$$\frac{1}{2} c_o' \frac{d}{dx}(u_s^3 D) = gD \frac{u_s}{\rho_n}\left[c_2 \beta \rho_n \frac{d}{dx}[D(T_s - T_n)] + (c_2 + c_3)\beta \rho_n (T_s - T_n)\frac{dD}{dx}\right]$$

$$- \frac{1}{\rho_n} u_s |\tau_o| S_j \tag{30}$$

$$c_4 \frac{d}{dx}(u_s (T_s - T_n) D) + \frac{\phi_n}{\rho_n c_p} = 0 \tag{31}$$

in which

$$c_o = \int_0^1 f^2 d\eta;\ c_o' = \int_o^1 f^3 d\eta,\ c_1 = \int_o^1 \int_\eta^1 h\, d\eta,\ c_2 = \int_o^1 f \int_\eta^1 h d\eta d\eta,$$

$$c_3 = \int_o^1 \eta \frac{\partial f}{\partial \eta} \int_\eta^1 h d\eta d\eta,\ c_4 = \int_o^1 f h d\eta,\ \int_o^1 f(\eta) \frac{\partial \bar{\tau}}{\partial \eta} d\eta = - S_j$$

in which S_j is a constant (j representing the flow regime as defined below) depending on the profiles for velocity and shear stress. Explicit expressions for S_j are given in a later section. The bottom shear stress, is modeled using

$$\frac{\tau_o}{\rho_n} = - F_{oj} \left(\frac{\nu}{D}\right)^{2-j} u_s^j \tag{32}$$

in which υ = kinematic viscosity of water; j = 1 when the flow in the lower layer is laminar; j = 2 when the flow in the lower layer is turbulent; and F_{o1} and F_{o2} are positive constants which depend only on parameters of the non-dimensional similarity profiles for velocity and temperature. Explicit expressions for F_{o1} and F_{o2} are given later. The notation j=1 represents both the laminar and quasi-laminar regimes. Surface heat loss is determined from the linearized relation

$$\phi_n = K(T_s - T_e) \tag{33}$$

where K is the surface heat-exchange coefficient and T_e is the equilibrium temperature. The following normalized variables are introduced.

$$\phi = \frac{u_s}{\sqrt{\beta(T_o - T_e) g D_o}}, \theta = \frac{T_s - T_n}{T_o - T_e}, \theta_n = \frac{T_n - T_e}{T_o - T_e}, \bar{D} = D/D_o, \xi = x/D_o \tag{34}$$

in which T_o is the water-surface temperature at x=0.

An order of magnitude analysis based on results of past numerical and analytical studies (Sturm 1976; Sturm 1981) indicates that the inertia term in the momentum equation is negligible compared to the other terms in most situations in the field and in the laboratory. On elimination of the inertia contribution in Eqs. 29 and 30 and substitution of Eqs. 32, 33, and 34, the governing equations become

Momentum:

$$\left[c_1\theta - \frac{1}{2\beta(T_o - T_e)}\right]\frac{d\bar{D}^2}{d\xi} + c_1\bar{D}^2\frac{d\theta}{d\xi} + \frac{F_{oj}\phi^j}{(\bar{D}\sqrt{G})^{2-j}} = 0 \tag{35}$$

Mechanical Energy:

$$\left(c_2 + \frac{c_3}{2}\right)\theta\frac{d\bar{D}^2}{d\xi} + c_2\bar{D}^2\frac{d\theta}{d\xi} - \frac{F_{oj}S_j\phi^j}{(\bar{D}\sqrt{G})^{2-j}} = 0 \tag{36}$$

Thermal Energy:

$$\bar{D}\frac{d}{d\xi}(\phi\theta) + \phi\theta\frac{d\bar{D}}{d\xi} - \frac{(\theta + \theta_n)}{c_4 P_m\sqrt{G}} = 0 \tag{37}$$

where

$$G = \frac{\beta(T_o - T_e)\, g D_o^3}{\nu^2}, P_m = \frac{\nu}{k D_o}, k = \frac{K}{\rho c_p}$$

Eqs. 35, 36 and 37 contain three dimensionless governing parameters: the Grashof number G, the modified Prandtl number P_m, and $\beta(T_o - T_e)$.

An expression for $\frac{d\bar{D}^2}{d\xi}$ may now be found by suitably manipulating the momentum and mechanical energy equations:

$$\frac{d\bar{D}^2}{d\xi} = \frac{\left[1 + \frac{c_1}{c_2}S_j\right] F_{oj}}{\left[\frac{1}{2}\beta\,(T_o - T_e) + \frac{c_3 c_1}{2c_2}\,\theta\right]} \frac{\phi}{(\bar{D}\sqrt{G})^{2-j}} \tag{38}$$

Eliminating $\frac{d\bar{D}^2}{d\xi}$ from Eqs. 35 and 36 gives

$$c_3 \frac{c_1}{2}\bar{D}^2\theta\frac{d\theta}{d\xi} + \frac{c_2}{2\beta(T_o-T_e)}\bar{D}^2\frac{d\theta}{d\xi} - \frac{S_j F_{oj}}{2\beta(T_o-T_e)}\frac{\phi^j}{(\bar{D}\sqrt{G})^{2-j}}$$

$$+ \frac{\theta\phi^j F_{oj}\{c_2 + \frac{c_3}{c_2} + c_1 S_j\}}{(\bar{D}\sqrt{G})^{2-j}} = 0 \tag{39}$$

Substituting Eq. 38 into the normalized thermal energy equation, Eq. 37, yields

$$\bar{D}^2\frac{d}{d\xi}(\phi\theta) + \frac{\theta\phi^{j+1}}{2}\frac{F_{oj}}{[\frac{1}{2}\beta(T_o-T_e) + \frac{c_3 c_1\theta}{2c_2}]}\frac{[1 + \frac{c_1}{c_2}S_j]}{(\bar{D}\sqrt{G})^{2-j}}$$

$$+ \frac{\bar{D}\,(\theta + \theta_n)}{c_4 P_m\sqrt{G}} = 0 \tag{40}$$

The simplified governing equations for the problem are Eqs. 38 to 40 which constitute three non-linear ordinary differential equations in the three unknowns, ϕ, θ and D.The magnitude of D is very nearly 1 as indicated by the numerical and analytical results of Sturm (1976, 1981); therefore, Eqs. 38 to 40 are further simplified by setting D = 1 in Eqs. 39 and 40. Eqs. 39 and 40 then become uncoupled from Eq. 38 and can be handled separately to yield the solutions for ϕ and θ The problem then reduces to finding a solution to the following system of two differential equations:

$$\gamma_1\theta\theta' + \gamma_2\theta' + \gamma_3\theta\phi^j - \gamma_4\phi^j = 0 \tag{41}$$

$$\theta\phi' + \theta'\phi + \frac{\gamma_5}{f_1(\theta)}\theta\phi^{j+1} + \gamma_6(\theta + \theta_n) = 0 \tag{42}$$

where

$$\gamma_1 = \frac{c_3 c_1}{2}, \gamma_2 = \frac{c_2}{2\beta(T_o - T_e)}, \gamma_3 = F_{oj} \frac{\{c_2 + \frac{c_3}{c_2} + c_1 S_j\}}{(\sqrt{G})^{2-j}},$$

$$\gamma_4 = \frac{S_j F_{oj}}{2\beta(T_o - T_e)(\sqrt{G})^{2-j}},$$

$$\gamma_5 = \frac{1}{2} F_{oj} \frac{[1 + \frac{c_1}{c_2} S_j]}{(\sqrt{G})^{2-j}},$$

$$\gamma_6 = \frac{1}{c_4 P_m \sqrt{G}} \quad \text{and} \quad f_1(\theta) = \frac{1}{2\beta(T_o - T_e)} + \frac{c_3 c_1 \theta}{2c_2} \tag{43}$$

and the primes denote differentiation with respect to ξ. Since the coefficients γ_1 through γ_6 and $f_1(\phi)$ do not contain the independent variable ξ explicitly, Eqs. 41 and 42 can be reduced to a single non-linear equation in ϕ and θ which is solved (see following section) using an internal condition for the flow to be well behaved in the sidearm. Therefore, only one boundary condition is required for the solution of Eqs. 41 and 42 and this is obtained from the condition that $T_s = T_o$ at $x = 0$. This boundary condition reduces in the normalized form to

$$\theta = (1 - \theta_n) \text{ at } \xi = 0 \tag{44}$$

Solution

Eqs. 41 and 42 can be suitably manipulated to obtain

$$\frac{d\phi}{d\theta} + \left\{ - \frac{\gamma_5}{f_1(\theta)} \cdot \left(\frac{\gamma_1 \theta + \gamma_2}{\gamma_3 \theta - \gamma_4} \right) + \frac{1}{\theta} \right\} \phi = \left\{ \frac{\gamma_6 (\theta + \theta_n)}{\theta} \left(\frac{\gamma_1 \theta + \gamma_2}{\gamma_3 \theta - \gamma_4} \right) \right\} \phi^{-j} \tag{45}$$

which is of the form

$$\frac{d\phi}{d\theta} + r(\theta)\, \phi = s(\theta)\, \phi^m \tag{46}$$

Eq. 46 is the Bernoulli equation (Ames 1968). An exact solution to Eq. 45 can therefore be found; however the complicated forms of the functions $r(\theta)$ and $s(\theta)$ make it impossible to arrive at explicit expressions for $\phi(\xi)$ and $\theta(\xi)$. Order of magnitude simplifications can be readily made in the parent governing equations 41 and 42 (Cherian 1985); these simplifications result from the fact that the factor $\beta(T_o - T_e)$ is at least two or three orders of magnitude smaller than unity. The simplified governing equations are

$$\gamma_2 \theta' - \gamma_4 \phi^j = 0 \tag{47}$$

$$\theta \phi' + \theta' \phi + \gamma_6 (\theta + \theta_n) = 0 \tag{48}$$

Eqs. 47 and 48 can also be reduced to the Bernoulli form with

$$r(\theta) = \frac{1}{\theta} \tag{49}$$

$$s(\theta) = -\frac{\gamma_6\gamma_2}{\gamma_4}\left(\frac{\theta + \theta_n}{\theta}\right) \tag{50}$$

$$m = -j \tag{51}$$

Eq. 46 can be solved using the transformation

$$\phi = t^{1/(1-m)} \tag{52}$$

The solution is given by

$$t = \exp\left[(m-1)\int r(\theta)\, d\theta\right]\left\{A-(m-1)\int s(\theta)\cdot\exp\left[(1-m)\int r(\theta)\, d\theta\right] d\theta\right\} \tag{53}$$

Substituting Eqs. 49, 50 and 51 in Eq. 53 yields

$$t = \theta^{-(j+1)}\left\{A - (j+1)\frac{\gamma_2\gamma_6}{\gamma_4}\theta^{j+1}\left(\frac{\theta}{j+2} + \frac{\theta_n}{j+1}\right)\right\} \tag{54}$$

The constant A must equal zero, because the velocity must remain finite when θ goes to 0; this is the internal condition (referred to earlier) for the flow to be well behaved in the sidearm. Thus the solution from Eqs. 52 and 54 is

$$\phi^{j+1} = \left[\theta + \frac{j+2}{j+1}\theta_n\right]/\delta_1 \tag{55}$$

in which

$$\delta_1 = -\frac{(j+2)}{(j+1)}\frac{\gamma_4}{\gamma_2\gamma_6} \tag{56}$$

From Eqs. 47 and 48,

$$\phi' = -(1/\theta)\{\phi^{(j+1)}\frac{\gamma_4}{\gamma_2} + \gamma_6(\theta + \theta_n)\} \tag{57}$$

Substitution for ϕ from Eq. 55 into Eq. 57 gives

$$\phi' = -\frac{\gamma_6}{j+2} \tag{58}$$

which on integration yields

$$\phi = (-\frac{\gamma_6}{j+2})\,\xi + B \tag{59}$$

in which B is a constant of integration. The value of B is obtained using the boundary condition in Eq. 44 which yields after use of Eq. 55,

$$B = \left[\left(1 + \frac{\theta_n}{j+1}\right)/\delta_1\right] \tag{60}$$

Hence the solution of the governing equations, Eq. 47 and 48, is given by

$$\phi = \left[\left(1 + \frac{\theta_n}{j+1}\right)/\delta_1\right]^{1/(j+1)} - (\gamma_6/j+2)\,\xi \tag{61}$$

$$\theta = \delta_1 \left[\left\{\left(1 + \frac{\theta_n}{j+1}\right)/\delta_1\right\}^{1/(j+1)} - (\gamma_6/j+2)\xi\right]^{j+1} - \frac{j+2}{j+1}\theta_n \tag{62}$$

The unknown θ_n is determined from Eq. 19 which can be written as,

$$\theta = 0 \text{ at } \xi = \bar{L} \tag{63}$$

in which $\bar{L} = L/D$. Eqs. 62 and 63 yield

$$0 = \delta_1 \left[\left(1 + \frac{\theta_n}{j+1}\right)/\delta_1\right]^{1/j+1} - (\gamma_6/j+2)\,\bar{L}\Big]^{j+1} - \frac{j+2}{j+1}\theta_n \tag{64}$$

Note that when $\bar{L} = \bar{L}_e$, $\theta_n = 0$, which when substituted in Eq. 64 yields an expression for $\bar{L}_e$

$$\bar{L}_e = \frac{(j+2)}{\gamma_6 \delta_1^{1/(j+1)}} \tag{65}$$

Using Eq. 65, Eq. 64 can be expressed as

$$\lambda = (1 + \frac{\theta_n}{j+1})^{1/j+1} - (\frac{j+2}{j+1}\theta_n)^{1/j+1} \tag{66}$$

in which $\lambda = \bar{L}/\bar{L}_e = L/L_e$. Using Eq. 66, θ_n can be expressed as

$$\theta_n = e_j(\lambda),\ j = 1,2 \tag{67}$$

in which e_1 and e_2 are functions of λ. When $j = 1$ (laminar and quasi-laminar sidearm flows),

$$e_1(\lambda) = 1 + \lambda\,[2\lambda - \sqrt{3\lambda^2 + 6}] \tag{68}$$

and when $j = 2$ (turbulent sidearm flow)

$$e_2(\lambda) = \frac{3}{4}(U + S - \frac{4}{3}\lambda)^3 \tag{69}$$

in which

$$U = \left(\frac{2}{9}\right)^{1/3} [(3 - \frac{5}{3}\lambda^3) + \sqrt{(9-\lambda^3)(1-\lambda^3)}]^{1/3} \quad (70)$$

and

$$S = \left(\frac{2}{9}\right)^{1/3} [(3 - \frac{5}{3}\lambda^3) - \sqrt{(9-\lambda^3)(1-\lambda^3)}]^{1/3} \quad (71)$$

The expression in Eq. 68 is the same as that obtained by Sturm (1981) and Jain (1982). Note that the boundary condition $\theta = 0$ at $\xi = \bar{L}$ implies that the maximum value of $\bar{L}$ is $\bar{L}_e$; hence $\lambda \leq 1$, a condition that was used in deriving Eq. 69.

A summary of the analytical solution is given below:

$$\theta = \left[\left(1 + \frac{\theta_n}{j+1}\right)^{1/j+1} - x/L_e\right]^{j+1} - \frac{j+2}{j+1} \cdot \theta_n \quad (72)$$

$$\phi = \left[\left(1 + \frac{\theta_n}{j+1}\right)^{1/j+1} - x/L_e\right] / \delta_1^{1/(j+1)} \quad (73)$$

where

$$\bar{L}_e = c_4 P_m \sqrt{G}\, (j+2)/\delta_1^{1/(j+1)} \quad (74)$$

$$\delta_1 = (c_4/c_2)((j+2)/(j+1))S_j F_{oj} P_m G^{(j-1)/2}$$

The rate of surface heat loss, H_L, from a unit width of a channel of length L is

$$H_L = \int_0^L K(T_s - T_e)\, dx \quad (75)$$

which on substitution for T_s from Eq. 72 and integration becomes

$$H_L = KL_e(T_o - T_e) \left[\frac{(1+\theta_n/j+1)}{j+2} - \frac{\theta_n \lambda}{j+1} - \frac{[(1+\theta_n/j+1)^{1/j+1} - \lambda]^{j+2}}{j+2}\right] \quad (76)$$

The rate of heat loss, H_{Le}, from a unit width of long channel [sidearm with a length $L \geq L_e$] is obtained by setting $\lambda = 1$ and $\theta_n = 0$ in Eq. 76

$$H_{Le} = K_{Le}(T_o - T_e)/(j+2) \quad (77)$$

The ratio

$$\eta_H = \frac{H_L}{H_{Le}} = (1 + \theta_n/j+1) - \frac{(j+2)}{(j+1)}\theta_n \lambda - [(1 + \theta_n/j+1)^{1/j+1} - \lambda]^{j+2} = f_j(\lambda) \quad (78)$$

The surface velocity is determined from Eq. 73 as

$$u_s/k\bar{L}_e = \frac{1}{(j+2)c_4} [(1 + \frac{\theta_n}{j+1})^{1/j+1} - \frac{x}{L_e}] \quad (79)$$

The flow rate, q, per unit width in the upper layer is

$$q = \int_{h_v}^{D} u\,dy = c_5\, u_s\, D_o \tag{80}$$

in which $c_5 = \int_{\Lambda_v}^{1} f(n)\, d\eta$ and D is set equal to D_o. Substituting for u_s from Eq. 79 leads to

$$\frac{q}{kL_e} = \frac{c_5}{(j+2)c_4}\left\{\left(1 + \frac{\theta_n}{j+1}\right)^{1/(j+1)} - x/L_e\right\} \tag{81}$$

The rate of continuous downflow, V, from the upper layer to the lower layer, obtained from Eq. 81 is

$$V = \frac{c_5}{(j+2)c_4} \tag{82}$$

The unit flow rate, q_o, at x = 0 given by Eq. 81 is

$$q_o/kL_e = \frac{c_5}{c_4(j+2)}\left(1 + \frac{\theta_n}{j+1}\right)^{1/(j+1)} \tag{83}$$

The unit discharge, q_{oe}, at x = 0 for a long channel is obtained by setting $\theta_n = 0$ in Eq. 83:

$$q_{oe}/kL_e = \frac{c_5}{(j+2)c_4} \tag{84}$$

The ratio

$$\eta_{qo} = q_o/q_{oe} = \left(1 + \frac{\theta_n}{j+1}\right)^{1/(j+1)} \tag{85}$$

The variation of θ_n, η_H and η_{qo} with λ is shown in figure 2 for the laminar/quasi-laminar and turbulent cases.

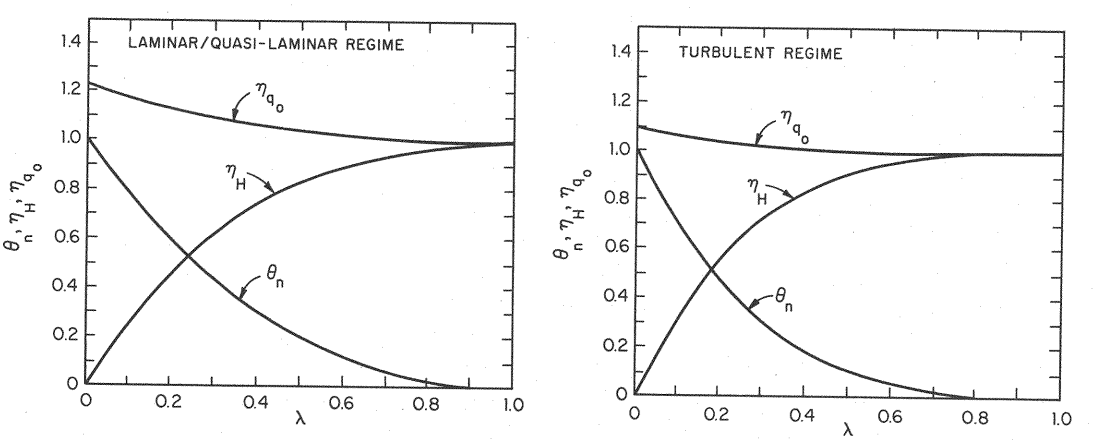

Figure 2. Variation of θ_n, η_H, η_{qo}.

COMPARISON WITH EXPERIMENTAL DATA

The analytical model involves certain constants which need to be evaluated in order to compare the model results with the experimental data.

Evaluation of Constants

F_{oj} in Eq. 32 is related to the friction factor at the channel bottom by the relation

$$\frac{\tau_o}{\rho_n} = -F_{oj}\left(\frac{\upsilon}{D}\right)^{2-j} u_s^{\,j} = \frac{f_{oj}}{8} U_L |U_L| \tag{86}$$

in which f_{oj} is the friction factor of the channel bottom and U_L is the average velocity of the lower layer. For laminar/quasi-laminar conditions, use of $f_{o1} = 48/R_e$, in which R_e is the Reynolds number of the lower layer, gives

$$F_{o1} = 6\left|\frac{c_6}{\Lambda_T^2}\right| \tag{87}$$

in which

$$c_6 = \int_o^{\Lambda_T} f(\eta)\, d\eta$$

For turbulent conditions, Eq. 86 gives

$$F_{o2} = \frac{f_{o2}}{8}\frac{c_6^2}{\Lambda_T^2} \tag{88}$$

where f_{o2} is a bottom friction factor for turbulent flow and depends primarily on the roughness of the channel bottom.

The evaluation of S_j in Eq. 30 requires an expression for the interfacial shear stress, τ_i, which is defined as

$$\frac{\tau_i}{\rho_n} = \frac{f_{ij}}{8}(U_U - U_L)^2 \tag{89}$$

in which f_{ij} is the interfacial friction factor and U_U is the average velocity in the upper layer. Introduce

$$\alpha_j = f_{ij}/f_{oj} \tag{90}$$

Then

$$\tau_i/|\tau_o| = \alpha_j\left(1 + \frac{\Lambda_T}{1-\Lambda_T}\right)^2 \tag{91}$$

There is some uncertainty with regard to the value of α_j. Interfacial friction in two-layer flows has been the subject of numerous investigations; however, past surveys of the literature (Vreugdenhil 1971; Karelse 1974; Maxwell et al. 1975) have failed to determine well-established universal relationships yielding f_{ij} as a function of the pertinent independent variables. There are a number of reasons why consistent correlations were not found in the data: 1) the variability among various

investigators in defining the velocity and length scales, and the associated lack of information required to bring all the data to a common base; 2) the sensitivity of the data analysis to quantities that cannot be measured accurately (like the water-surface and interfacial slopes); and 3) the lack of systematic variation of the Reynolds and densimetric Froude numbers over a wide range of values. Another major reason for the inconsistency in the experimental data is that it pertains to a variety of two-layer flows (temperature wedges, saline wedges, lock-exchange flows, gravity underflows, etc.). In the different types of two-layer flows, different processes contributing to interfacial friction might dominate, thereby leading to different relationships for f_{ij}. In general, the processes affecting interfacial friction are: 1) laminar viscous friction; 2) internal wave form drag; 3) drag caused by interfacial wave breaking and entrainment; and 4) Reynolds stress of turbulent motion. In the case of sidearm flow in which surface cooling plays a major role, a fifth process may be important: convective turbulence. In the quasi-laminar and turbulent range of sidearm flow, convective turbulence is a dominant physical process in the upper layer and may influence the value of f_{ij}.

The data in the laminar range obtained by Barr (1967) was analyzed by Abraham and Eysink (1971), the results of which showed that α_1 varied between 0.5 and 1.0, with an average value of about 0.7. A theoretical model developed by Brocard et al. (1978) for equal counterflow indicates that $\alpha_1 \cong 0.2$. One reason for this discrepancy between laboratory data and the analytical result may be the significant contributor to interfacial friction at low Reynolds number. Macagno and Rouse (1962) have observed the existence of interfacial waves in the laminar range. An average value of $\alpha_1 \cong 0.5$ is best representative for the laminar range. In the turbulent range, an interpretation by Abraham et al. (1979) of the results of stability analysis for three-layer flow by Dingemans (1972) indicated that interfacial friction is a function only of the Reynolds number and the type of flow. Analysis of the data of Abraham and Eysink (1971) showed that α_2 varied from 0.27 to 0.39 with an average value of 0.35. The value of α_2 in sidearm flow should be higher because convective turbulence (which plays a dominant role in the quasi-laminar and turbulent regimes) contributes to increased momentum transfer across the interface. Therefore,α_2 is increased arbitrarily to 0.5. Similarly, for the quasi-laminar regime the value ofα_1 should be greater than 0.5 (the value for laminar flow); increasing a1 by about the same percentage as α_2 results in $\alpha_1 = 0.75$ for quasi-laminar flow.

There is some empiricism in the selection of the average values of α_j determined above; they are, however, based on the best available information and conform to the range of α_j (between 0.5 and 1.0) encountered in both laboratory and field studies.

Determination of the profile parameters Λ_T and Λ_V ,and the constants c_1 through c_6, and S_j requires knowledge of the similarity profiles for velocity, temperature, and shear stress. No satisfactory theoretical model is as yet available to predict the vertical distributions of velocity, temperature, and shear stress. Consequently, recourse is taken to examining the available experimental data to determine the appropriate similarity profiles. The examination of the results of laboratory investigations on sidearm flow indicates that Λ_T is not significantly different from Λ_V in the well-established flow region. It is therefore assumed that $\Lambda_T = \Lambda_v = \Lambda$.

Similarity profiles for velocity and temperature for each regime are identified using available experimental data and physical reasoning, and are shown in figure 3. It should be noted that the profiles are chosen to satisfy boundary conditions, Eqs. 20 to 27. Algebraic expressions for these profiles and profile constants are given in a report by Cherian and Jain (1985). The similarity profiles for the laminar regime are based on the experimentally obtained distributions of velocity and temperature given by Sturm. On the basis of the experimental results of Brocard et al. (1977) a similarity profile for velocity for the quasi-laminar regime is chosen such that the velocity is uniform in the upper layer and has a parabolic shape (representative of laminar flow) in the lower layer. The similarity profile for temperature is developed using a uniform distribution in the upper layer and a second-order temperature decay in the lower layer. No experimental data on the velocity and temperature distributions are available for the turbulent regime in sidearm flows; however, these distributions can be expected to have turbulent, well-mixed characteristics and are therefore best represented by a uniform profile in both layers.

No experimental data are available for the vertical distribution of shear stress. In view of the uncertainty in estimating the value of α_j, which is judged to be more important than the shape of the shear-stress profile, a linear profile for shear stress shown in figure 4, which satisfies the boundary conditions given by Eq. 28, is assumed. The constant S_j in Eq. 30, for the assumed shear-stress profile, can be written as

$$S_j = c_6 \left\{ \frac{(1-\Lambda_T) + \alpha_j/(1-\Lambda_T)^2}{\Lambda_T(1-\Lambda_T)} \right\} \qquad (92)$$

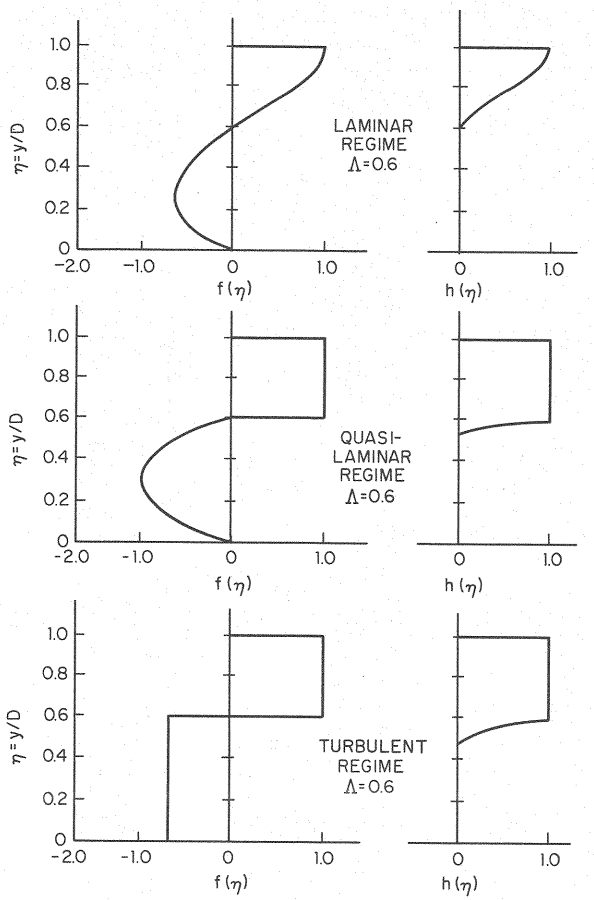

Figure 3. Similarity Profiles for Velocity and Temperature.

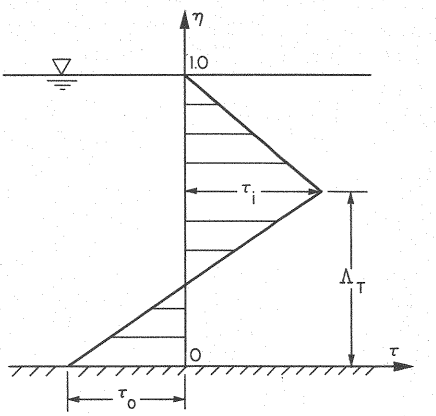

Figure 4. Shear Stress Distribution.

It is emphasized that the general behavior of density currents predicted by the present analysis does not depend on the assumed profiles for velocity temperature, and shear stress. The reasonableness of the assumed profiles is confirmed by the satisfactory agreement between the analytical results and experimental data as presented below.

The laminar model developed herein is applied to the experimental data for Run B of Sturm (1976). The experimental and computed values of θ_n and q_o/kL are 0.54 and 0.52, and 1.84 and 2.27, respectively. The agreement is satisfactory, even though the model overpredicts the sidearm discharge by about 25%. The experimental results of Brocard et al. (1977) are used to verify the quasi-laminar model. The data were screened to exclude results from runs in which Λ was greater than 0.65 or less than 0.55 (indicative of flow that was not well-established). The results of the data comparison are shown in figures 5 and 6. Field data is available from the Boundary Dam Reservoir, Saskatchewan, Canada (Brocard et al. 1977). Seventy-seven percent of the reservoir surface area consists of a long and narrow sidearm. The length of the sidearm is 37,000 ft and its depth at the entrance is 60 ft. Surface temperatures were measured at the sidearm entrance and at a longitudinal distance of 21,000 ft from the sidearm entrance. Model predictions for $(T_x - T_e)/(T_o - T_e)$, in which T_x is the surface temperature measured at x = 21,000 ft from the sidearm entrance, are generated using the equations for the turbulent case. The results are shown in figure 7. Overall, the models developed herein perform fairly well, as is demonstrated by the above comparisons.

A graphical comparison for q_o/kL in the laminar regime using various models is shown in figure 8. Figure 9 depicts the comparison for θ_n in the laminar regime. The temperature profile used in generating Sturm's result is $h(\eta) = \eta^4$ which best resembled the similarity profile for temperature in the laminar regime. The wide discrepancy between the results of the present model and that of Jain

(1982) is primarily due to the neglect, in his model, of the water-surface slope term in the momentum equation. The water-surface slope term (the first term in Eq. 35) is more important than the bottom-friction term (the third term in Eq. 35). Taking the ratio of these terms, substituting for $dD^2/d\xi$ from Eq. 38, and using the order of magnitude approximations $1/[\beta\,(T_o - T_e)] >> c_1$, θ and $1/[\beta\,(T_o - T_e)] >> c_3c_1\theta/2c_2$, the following is obtained:

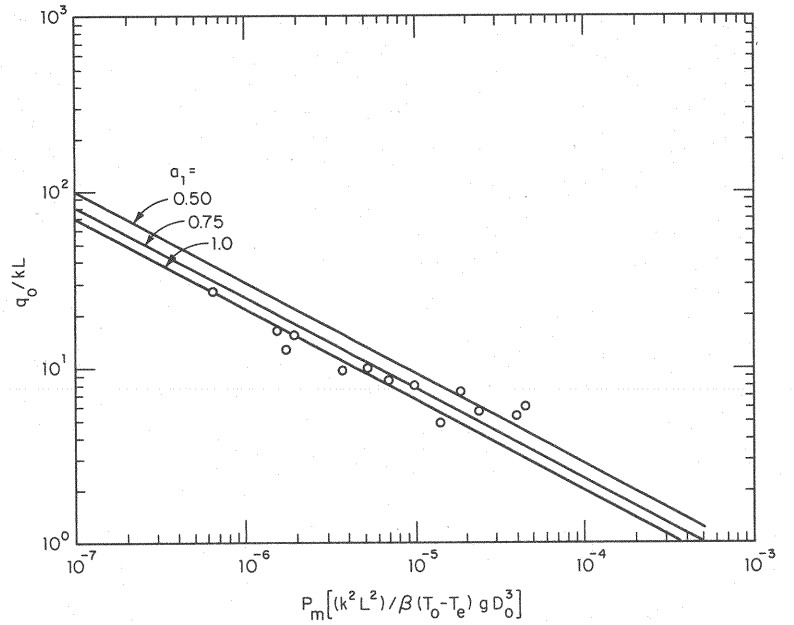

Figure 5. Comparison of Predicted q_o/kL with Data of Brocard et al. (1977).

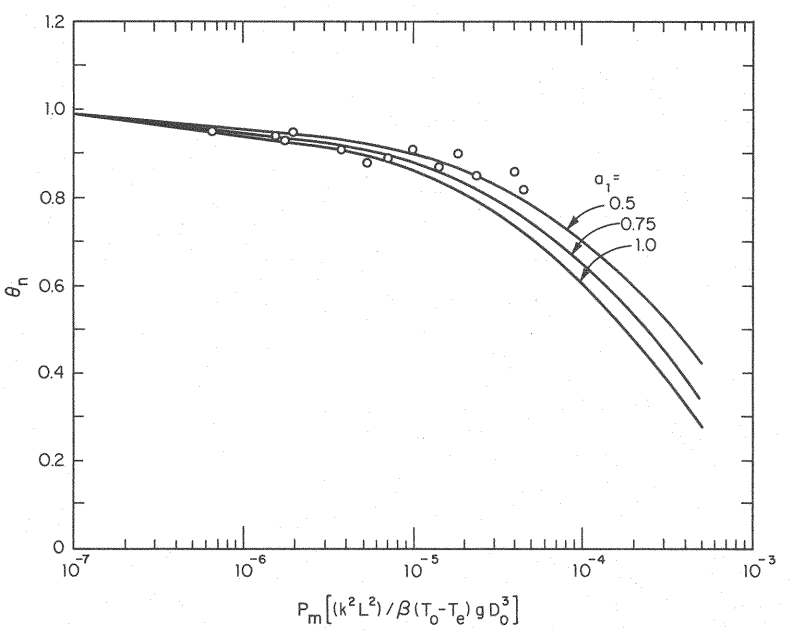

Figure 6. Comparison of Predicted θ_n with Data of Brocard et al. (1977).

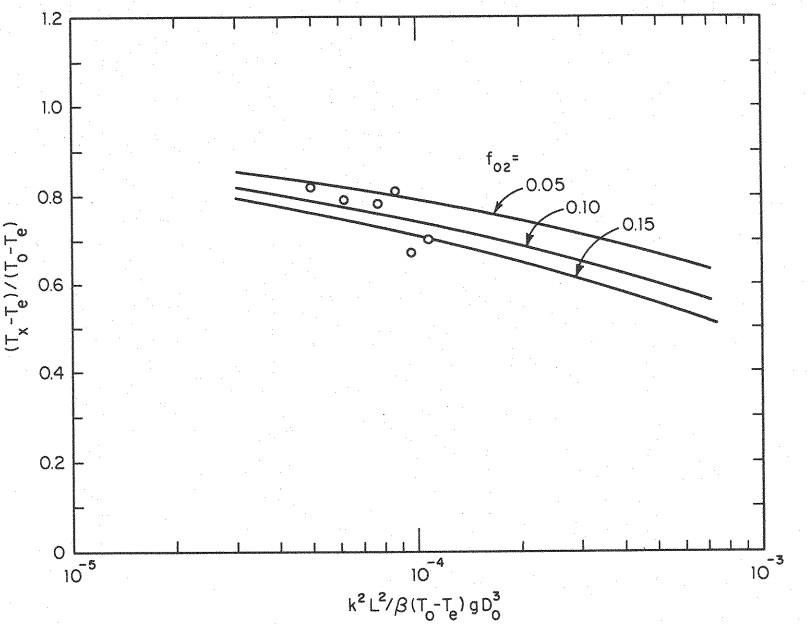

Figure 7. Comparison with Boundary Dam Data.

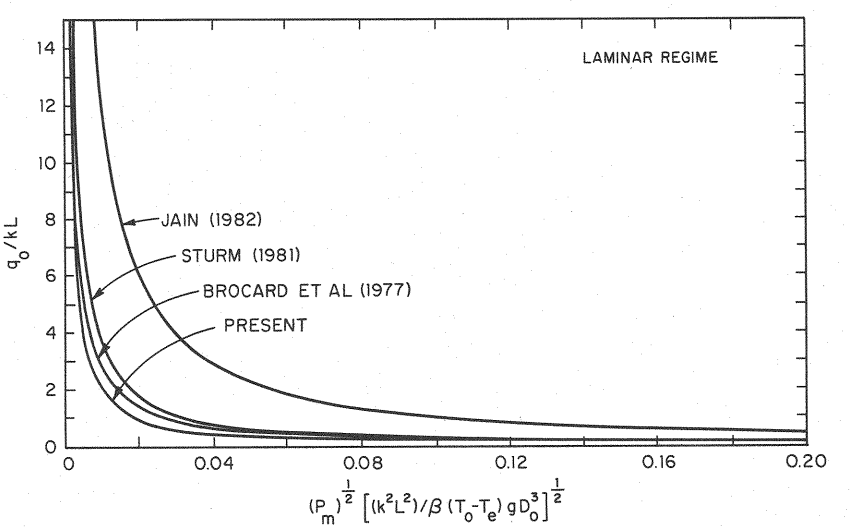

Figure 8. Comparison of Analytical Solutions for q_o/kL.

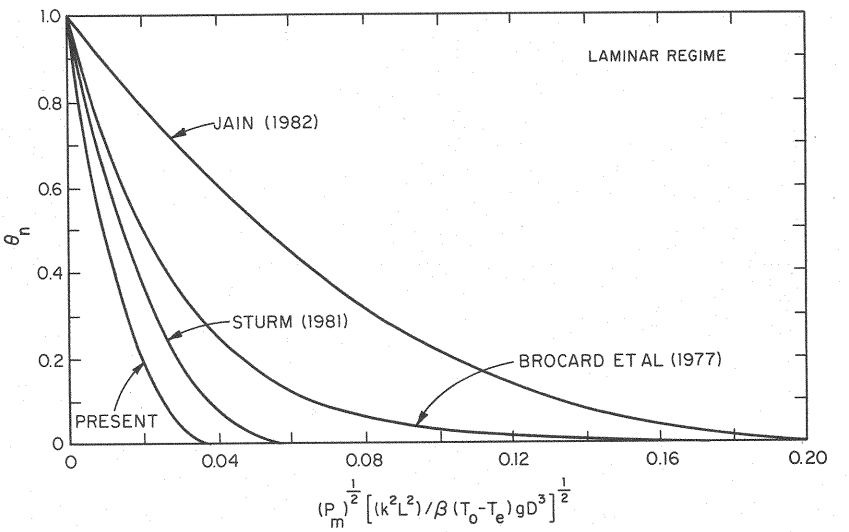

Figure 9. Comparison of Analytical Solutions for θ_n (Laminar Regime).

$$\frac{\text{contribution of water-surface slope term}}{\text{contribution of bottom-friction term}} = \left(1 - \frac{c_1}{c_2} S_j\right) \tag{93}$$

Based on the assumed profiles for velocity, temperature and shear-stress, the ratio of the two terms in Eq. 93 is more than 20. Comparison for θ_n in the turbulent regime is shown in figure 10. A comparison for q_o/kL in the turbulent regime showed that the solution of Brocard et al. overpredicts q_o/kL in comparison to the present solution by 13% to 25% (Cherian, 1985).

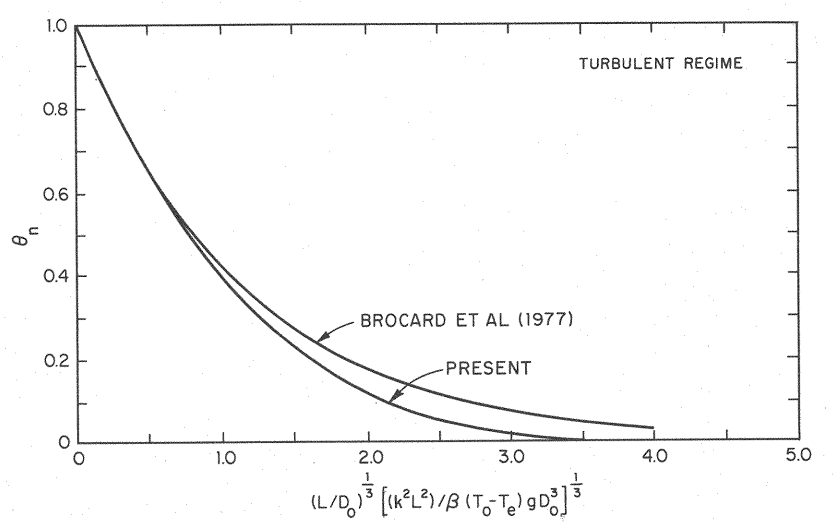

Figure 10. Comparison of Analytical Solutions for θ_n (Turbulent Regime).

CONCLUSIONS

The analytical solution indicates that the surface discharge in the sidearm decreases linearly along the length of the sidearm for both the laminar and turbulent cases, while the surface temperature decay is quadratic along the sidearm for the laminar case, and cubic along the sidearm for the turbulent case. The solution indicates that the water-surface slope is a significant factor in the depth-integrated momentum equation, and that the bottom friction plays a minor role in fully-established sidearm flow. The agreement between the analytical model and the experimental data is satisfactory.

APPENDIX I - REFERENCES

1. Abraham, G., Karelse, M., and Van Os, A.G., "On the Magnitude of Interfacial Shear of Subcritical Stratified Flow in Relation with Interfacial Stability", Journal of Hydraulic Research, Vol. 17, No. 4, 1979.

2. Abraham, G., and Eysink, W.D., "Magnitude of Interfacial Shear in Exchange Flow", Journal of Hydraulic Research, Vol. 9, No. 2, 1971.

3. Ames, W.F., "Nonlinear Ordinary Differential Equations in Transport Processes", Academic, 1968.

4. Barr, D.I.H., "Densimetric Exchange Flow in Rectangular Channels, III: Large-Scale Experiments", La Houille Blanche, 6, 1967.

5. Brocard, D.N., Jirka, G.H., and Harleman, D.R.F., "A Model for the Convective Circulation in Sidearms of Cooling Lakes", Report No. 223, Ralph M. Parsons Laboratory of Civil Engineering, Massachusetts Institute of Technology, 1977.

6. Cherian, M.P., "An Analytical Solution for Buoyancy-Driven Flow in Sidearms of Cooling Lakes", Ph.D. Thesis, Department of Civil and Environmental Engineering, University of Iowa, 1985.

7. Cherian, M.P., and Jain, S.C., "An Analytical Solution for Buoyancy-Driven Flow in Sidearms of Cooling Lakes", IIHR Report No. 286, May, 1985.

8. Dingemans, M.P., "Stability of Three Layer Flow", Report S57, Delft Hydraulics Laboratory, Delft, Netherlands, 1972.

9. Dresner, L., "One Dimensional Analysis of Heat Dissipation in a Side Arm of a Cooling Lake", Report TM-4287 Oak Ridge National Laboratory, Oak Ridge, Tennessee, 1973.

10. Edinger, J.E., "Shape Factors for Cooling Lakes", Journal of Power Division, ASCE, Vol. 97, No. P04, 1971.

11. Jain, S.C., "Buoyancy-Driven Circulation in Free-Surface Channels", Journal of Fluid Mechanics, Vol. 122, 1982.

12. Karelse, M., "Vertical Exchange Coefficients in Stratified Flows", Chapter 2. "Momentum and Mass Transfer in Stratified Flows", Delft Hydraulic Laboratory Report R880, Delft, Netherlands, 1974.

13. Kline, S.J., Morkovin, M.V., Sovran, G., and Cockrell, D.J., Proceedings of Computation of Turbulent Boundarty Layers - 1968 AFOSR-IFP-Stanford Conference, Vol. 1, Stanford University, Stanford, California, 1968.

14. Macagno, E.O. and Rouse, H., "Interfacial Mixing in Stratified Flow", Transactions ASCE, Vol. 127, 1962.

15. Maxwell, W.H.C., Holley, E.R., Lin, C.Y., and Tekeli, S., "Study of Stratified Overflows and Underflows", Research Report No. 98, University of Illinois at Urbana-Champaign, Water Resources Center, 1975.

16. Phillips, O.M., "On Turbulent Convection Currents and the Circulation of the Red Sea", Deep Sea Reserach, Vol. 13, 1966.

17. Reynolds, W.C., "A Morphology of the Prediction Methods," Proceedings of the 1968 AFSOR-IFP-Stanford Conference, Vol. 1, Stanford University, Stanford, California, 1968.

18. Sturm, T.W., "An Analytical and Experimental Investigation of Density Current in Sidearms of Cooling Ponds", Ph.D. Thesis, Department of Mechanics and Hydraulics, University of Iowa, 1976.

19. Sturm, T.W., "Laminar Gravitational Convection of Heat in Dead-End Channels", Journal of Fluid Mechanics, Vol. 110, 1981.

20. Sturm, T.W. and Kennedy, J.F., "Heat Loss from Sidearms of Cooling Lakes", Journal of the Hydraulics Division, Vol. 106, No. HY5, May 1980.

21. Vrengdenhil, C.B., "Friction Coefficients on the Interface of a Two-Layer System", Delft Hydraulics Laboratory, Internal Information Report No. V204, Delft, Netherlands, 1971.

(Received June 4, 1990; revised October 8, 1990)